

## Chapter 2

# Characteristics of Shale Reservoirs

### 2.1 Introduction

Shale gas reservoir shows several features dissimilar with conventional reservoir which make it difficult to understand behavior of it. In this chapter, these features such as natural fracture system, adsorption/desorption of gas, diffusion in nanopores, non-Darcy flow, and stress-dependent compaction are presented. In general, shale gas reservoir includes natural fractures which are believed to play a significant role in hydraulic fracture propagation and gas production. Pressure behavior of dual porosity model used to simulate the natural fracture system is presented. In shale reservoirs, hydrocarbon gas is stored in two ways which are free gas in the pore media and absorbed gas in the surface of organic material. Previous studies presented that gas desorption contribute 5–30 % of total gas production in shale reservoir. In order to simulate gas production in shale gas reservoirs, an accurate model of gas adsorption is very important. According to the International Union of Pure and Applied Chemistry (IUPAC) standard classification system, there are six different types of adsorption. Among these, Langmuir isotherm and BET isotherm are suitable for shale formation so that they are presented. Due to the presence of nanopores, fluid flow in shale reservoir cannot be calculated from Darcy equation. This phenomenon can be explained by the concept of slip flow and a common way to model the flow of gas in nanopore is to modify the no-slip boundary condition in continuum models by accounting for a slip boundary condition. Several studies are suggested for accurate diffusion modeling of shale reservoir. Darcy equation is also cannot applied to hydraulic fractures due to high velocity of gas flow. When the gas velocity increases significant inertial (non-Darcy) effects can occur. This induces an additional pressure drop in the hydraulic fractures in order to maintain the production rate. For simulate this mechanism, Forchheimer equation which can replace

the Darcy equation is used. The conductivity of fracture network in shale reservoir is sensitive to the stress-dependent compaction effect. Change of porosity and permeability due to change of stress and strain should be considered. Effect of shale rock compaction can be considered by several stress-dependent correlations coupled with geomechanical model.

## 2.2 Natural Fracture System

A naturally fractured reservoir has been referred to as dual porosity system because two types of porous regions that present distinctly different properties are in presence (Barenblatt et al. 1960). The first region forms the continuous system connected with the wells, whereas the second region only feeds fluid locally to the first region. These regions represent matrix and fractures which have different fluid storage and conductivity characteristics in shale gas reservoirs.

Warren and Root (1963), who idealized the system as an orthogonal set of intersecting fractures and cubic matrix blocks (Fig. 2.1), invoked a simple pseudo-semi-steady-state (PSSS) model of transfer from matrix to fractures. Figure 2.2 shows the early part of fundamental pressure response of Warren and Root (1963)'s dual porosity model in semi-log plot (Stewart 2011). Pressure behavior is characterized by the first straight line, a transition which looks like a straight line of nearly a zero slope, and a final straight line displaying the same slope as the first. The first straight line usually shows very short duration and represents the fracture system alone. The equations of this line are

**Fig. 2.1** Naturally fracture reservoir model composed of an orthogonal set of intersecting fractures and cubic matrix blocks

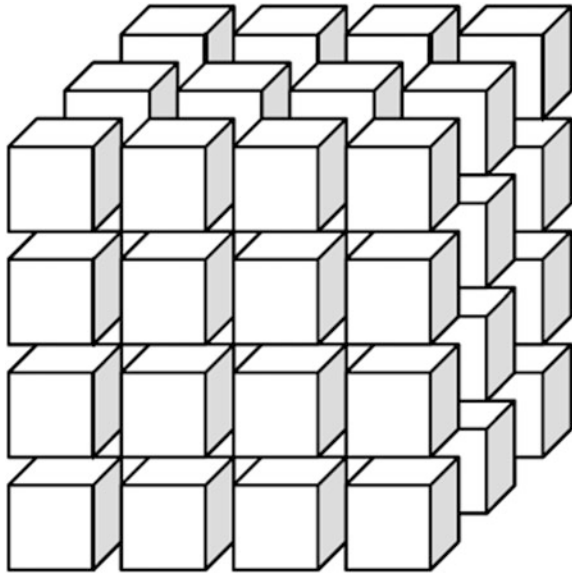
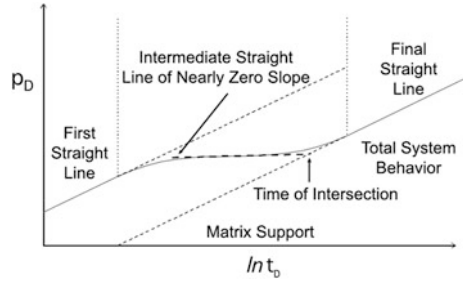


**Fig. 2.2** Dual porosity construction on a semi-log graph (Stewart 2011)



$$p_{wD} = \frac{1}{2}(\ln t_D) - \ln \omega + \ln \frac{4}{\gamma} \text{ or} \quad (2.1)$$

$$p_{wf} = p_i - \frac{q_{sc} B \mu}{4\pi k_{fb} h} \left( \ln t + \ln \frac{4k_{fb}}{\phi_{fb} c_f \mu r_w^2 \gamma} \right) \quad (2.2)$$

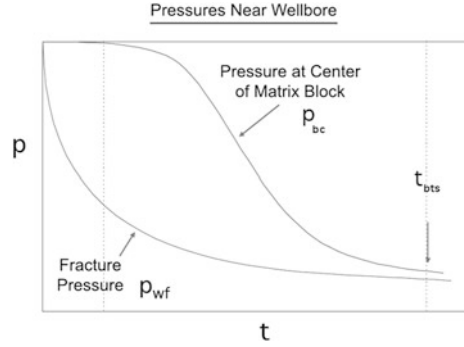
where  $p_{wD}$  is the dimensionless well flowing pressure,  $t_D$  the dimensionless time,  $\omega$  the dimensionless storativity,  $\gamma$  the exponential of Euler's constant, 1.781 or  $e^{0.5772}$ ,  $p_{wf}$  the well flowing pressure  $p_i$  the initial reservoir pressure  $q_{sc}$  the rate at standard condition,  $B$  the formation volume factor,  $\mu$  the viscosity,  $k_{fb}$  the bulk fracture permeability,  $h$  the net pay thickness,  $t$  the time,  $\phi_{fb}$  the bulk fracture porosity,  $c_f$  the formation compressibility, and  $r_w$  the well radius. The final straight line represents total system behavior and the equations of this period are given by

$$p_{wD} = \frac{1}{2} \left( \ln t_D + \ln \frac{4}{\gamma} \right) \text{ or} \quad (2.3)$$

$$p_{wf} = p_i - \frac{q_{sc} B \mu}{4\pi k_{fb} h} \left[ \ln t + \ln \frac{4k_{fb}}{(\phi c_t)_{m+f} \mu r_w^2 \gamma} \right] \quad (2.4)$$

where  $c_t$  is the total compressibility. Subscripts  $m$  and  $f$  indicate matrix and natural fracture. The separation between the lines is  $\ln \omega$ , which becomes larger in absolute value as  $\omega$  become smaller. In Fig. 2.3, fracture and matrix pressures which present a good insight into the mechanism of dual porosity behavior have been illustrated (Stewart 2011). At very early time, initial fracture and matrix pressures are same, whereupon support flow from the matrix is negligible. As the pressure transient propagates out from the well, fracture pressure declines quickly and matrix pressure declines slowly due to difference of conductivity. The flattening of semi-log graph is due to this period increasing support from the matrix to fracture. Depending on slowing down the rate of change of the fracture pressure and catching up of the matrix pressure, the two pressures are nearly analogous. Total system behavior is reached when the media pressures attain this dynamic equilibrium.

**Fig. 2.3** Fracture and matrix pressure in the natural fracture system (Stewart 2011)



### 2.3 Adsorption

The organic matter in shale has a strong adsorption potential due to the large surface area and affinity to methane (Yu et al. 2014). In order to simulate gas production in shale gas reservoirs, an accurate model of gas adsorption is very important. According to the standard classification system of the International Union of Pure and Applied Chemistry (IUPAC) (Sing et al. 1985), there are six different types of adsorption, as shown in Fig. 2.4. The shape of the adsorption isotherm is closely related to the properties of adsorbate and solid adsorbent, and on the pore-space geometry (Silin and Kneafsey 2012). The detailed description of the six isotherm classifications can be found in Sing et al. (1985).

**Fig. 2.4** Types of physical sorption isotherm (Sing et al. 1985)

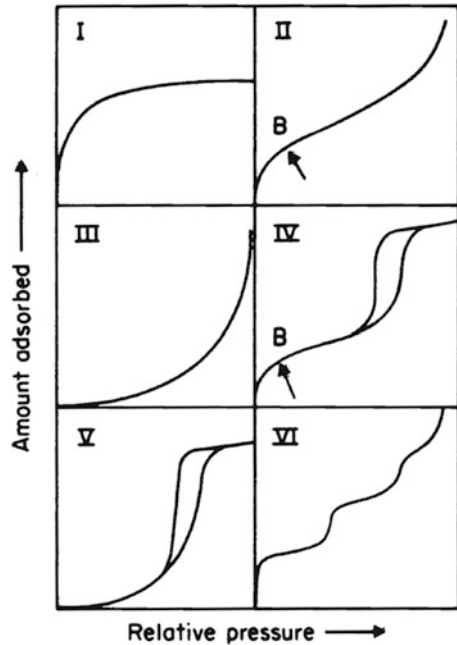
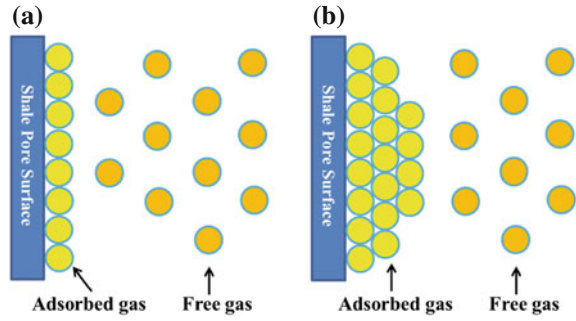


**Fig. 2.5** The schematic plots of monolayer and multilayer gas adsorption (Yu et al. 2014). **a** Monolayer Langmuir adsorption **b** Multilayer BET adsorption



The most commonly applied adsorption model for shale gas reservoirs is the classic Langmuir isotherm (Type I) (Langmuir 1918), which is based on the assumption that there is a dynamic equilibrium at constant temperature and pressure between adsorbed and non-adsorbed gas. Also, it is assumed that there is only a single layer of molecules covering the solid surface, as shown in Fig. 2.5a. The Langmuir isotherm has two fitting parameters as shown below:

$$V = \frac{V_L p}{p + p_L}, \quad (2.5)$$

where  $V$  is the gas volume of adsorption at pressure  $p$ ,  $V_L$  the Langmuir volume or the maximum gas volume of adsorption at the infinite pressure, and  $p_L$  the Langmuir pressure, which is the pressure corresponding to one-half Langmuir volume. Instantaneous equilibrium of the sorbing surface and the storage in the pore space is assumed to be established for the Langmuir isotherm (Freeman et al. 2012). Gao et al. (1994) demonstrated that the instantaneous equilibrium is a reasonable assumption because the ultra-low permeability in shale leads to very low gas flow rate through the kerogen component of shale.

At high reservoir pressures, one can expect that natural gas sorbed on the organic carbon surfaces forms multi-molecular layers. In other words, the Langmuir isotherm may not be a good approximation of the amount of gas sorbed on organic carbon-rich mudrocks. Instead, multilayer sorption of natural gas should be expected on organic carbon surfaces, and the gas adsorption isotherm of Type II should be a better choice. Type II isotherm often occurs in a non-porous or a macroporous material (Kuila and Prasad 2013). Brunauer et al. (1938) suggested the BET isotherm model which is a generalization of the Langmuir model to multiple adsorbed layers, as shown in Fig. 2.5b. The expression is shown as follows:

$$V_L = \frac{V_m C p}{(p_o - p) \left[ 1 + \frac{(C-1)p}{p_o} \right]} \quad (2.6)$$

where  $V_m$  is the maximum adsorption gas volume when the entire adsorbent surface is being covered with a complete monomolecular layer,  $C$  a constant related to the net heat of adsorption, and  $p_o$  the saturation pressure of the gas.  $C$  is defined as below:

$$C = \exp\left(\frac{E_1 - E_L}{RT}\right), \quad (2.7)$$

where  $E_1$  is the heat of adsorption for the first layer,  $E_L$  the heat of adsorption for the second and higher layers and is equal to the heat of liquefaction,  $R$  the gas constant, and  $T$  the temperature. The assumptions in the BET theory include homogeneous surface, no lateral interaction between molecules, and the uppermost layer is in equilibrium with gas phase. A more convenient form of the BET adsorption isotherm equation is as follows:

$$\frac{p}{V(p_o - p)} = \frac{1}{V_m C} + \frac{C - 1}{V_m C} \frac{p}{p_o} \quad (2.8)$$

A plot of  $\frac{p}{V(p_o - p)}$  against  $\frac{p}{p_o}$  should give a straight line with intercept of  $\frac{1}{V_m C}$  and slope of  $\frac{C-1}{V_m C}$ . Based on  $V_m$ , the specific surface area can be calculated using the following expression:

$$S = \frac{V_m N a}{22,400} \quad (2.9)$$

where  $S$  is the specific surface area in  $\text{m}^2/\text{g}$ ,  $N$  the Avogadro constant (number of molecules in one mole,  $6.023 \times 10^{23}$ ),  $a$  the effective cross-sectional area of one gas molecule in  $\text{m}^2$ , and 22,400 is the volume occupied by one mole of the adsorbed gas at standard temperature and pressure.

The standard BET isotherm assumes that the number of adsorption layers is infinite. But, in the case of  $n$  adsorption layers in some finite number, then a general form of BET isotherm is given below:

$$V(p) = \frac{V_m C \frac{p}{p_o}}{1 - \frac{p}{p_o}} \left[ \frac{1 - (n+1) \left(\frac{p}{p_o}\right)^n + n \left(\frac{p}{p_o}\right)^{n+1}}{1 + (C-1) \frac{p}{p_o} - C \left(\frac{p}{p_o}\right)^{n+1}} \right] \quad (2.10)$$

where  $n$  is the maximum number of adsorption layers. When  $n = 1$ , Eq. 2.10 will be reduced to the Langmuir isotherm, Eq. 2.5. When  $n = \infty$ , Eq. 2.10 will be reduced to Eq. 2.6.

Figure 2.6 compares shapes of the Langmuir and BET isotherms. Gas desorption along the BET isotherm contributes more significantly at early time of production than that with the Langmuir isotherm curve. This is because the slope of the BET isotherm curve at high pressure is larger than that of the Langmuir isotherm curve,

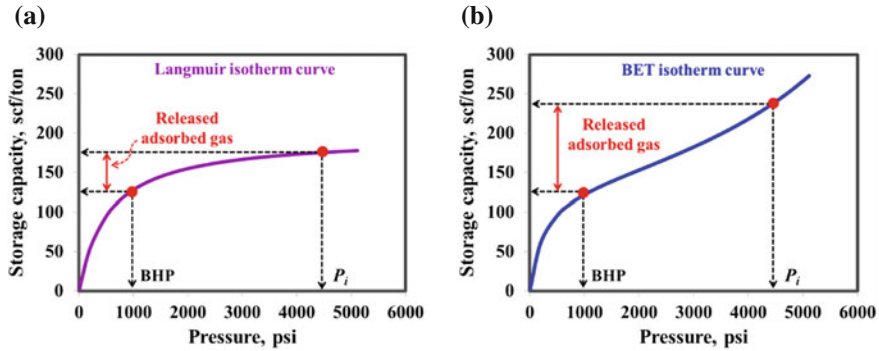


**Fig. 2.6** Comparison of the Langmuir and BET isotherms (Yu et al. 2014). **a** Langmuir isotherm **b** BET isotherm

resulting in more adsorbed gas releasing at early production times. In addition, under the same pressure drop from the initial reservoir pressure to the bottomhole pressure, the amount of released adsorbed gas with the BET isotherm curve is larger than that with the Langmuir isotherm curve.

## 2.4 Diffusion

The Darcy equation has been used for more than 150 years to linearly relate fluid-flow rate and pressure gradient across a porous system. The linearity of the Darcy equation makes it easy and practical to use in reservoir engineering analysis and numerical reservoir simulations. However, physics of fluid flow in shale reservoirs cannot be predicted from standard flow or mass transfer models because of the presence of nanopores, ranging in size from one to hundreds of nanometers, in shales. Conventional continuum flow equations, Darcy's law, greatly underestimate the flow rate when applied to nanopore-bearing shale reservoirs.

In other to articulate this phenomenon, Brown et al. (1946) suggested the concept of slip flow, which provided an explanation for the observed relationship between gas flow rate and mean pressure. As mentioned earlier, the pores in producing shale gas reservoirs are in the range of 1–100 nm so that the gas molecules contained in the pores are of comparable size ( $\sim 0.5$  nm). Under certain pressure and temperature conditions, the distance between gas molecules (mean free path) exceeds the size of the pores. In such conditions, the gas molecules might move singly through the pores and the concept of continuum and bulk flow may not be applicable. Knudsen number,  $K_n$ , is the ratio of mean free path,  $\lambda$ , to pore diameter,  $d$ , and can be used to identify different flow regimes in the porous media as given below

**Table 2.1** Different flow regimes as a function of Knudsen number (Rezaee 2015)

Knudsen number ( $K_n$ )	Flow regime
$0-10^{-3}$	Continuum/darcy flow (no-slip flow)
$10^{-3}-10^{-1}$	Slip flow
$10^{-1}-10^1$	Transition flow
$10^1-\infty$	Free-molecule flow

$$K_n = \frac{\lambda}{d}, \quad (2.11)$$

where

$$\lambda = \frac{k_B T}{\sqrt{2} \pi \delta^2 p}, \quad (2.12)$$

in which  $k_B$  is the Boltzmann constant and  $\delta$  is the collision diameter of the gas molecule. Table 2.1 presents flow regimes corresponding to Knudsen number ranges (Rathakrishnan 2004; Rezaee 2015). Continuum no-slip flow or Darcy equation is valid for  $K_n < 10^{-3}$ . Continuum flow with slip correction (Klinkenberg) is valid for  $K_n < 10^{-1}$ , which covers most conventional gas reservoirs and many tight gas reservoir conditions as well. However, as a result of the existence of nanopores in shales, the molecular mean free path becomes comparable with the characteristic geometric scale and  $K_n$  could be larger than 0.1. Under this condition, Knudsen diffusion, in addition to correction for the slip boundary condition, becomes the dominant mechanism and hence new forms of gas flow equations are needed. Various gas flow models for slip flow and Knudsen diffusion will be introduced in this section.

Klinkenberg (1941) showed experimentally that a linear relationship exists between Darcy permeability and the reciprocal of mean pressure in the system, that is, between gas-flux reduction and mean pressure increase.

$$k(p_{\text{avg}}) = k_D \left( 1 + \frac{b}{p_{\text{avg}}} \right), \quad (2.13)$$

where  $k(p_{\text{avg}})$  is the gas permeability at mean pressure ( $p_{\text{avg}}$ ),  $k_D$  the Darcy permeability or liquid permeability, and  $b$  the Klinkenberg parameters. The empirical parameters  $b$  and  $k_D$  are the slope and intercept of the fitted line through the  $k(p_{\text{avg}})$  versus  $\frac{1}{p_{\text{avg}}}$  data. The Klinkenberg effect has been used to model the gas flow in conventional gas reservoirs (with pores in the range of 10–100  $\mu\text{m}$ ) and recently for tight gas systems (with pores of 1–10  $\mu\text{m}$  in size).

The flow of gas in micro- or nanochannels can be described by use of molecular models, commonly known as molecular dynamics, which consider the molecular nature of a gas (Gad-el-Hak 1999) or Lattice-Boltzmann method (Shabro et al. 2012). Although these molecular models are valid for any range of  $K_n$ , the



requirement of large computational time and power constitutes a major limitation of these approaches, currently rendering them unfeasible for shale analysis. A common way to model the flow of gas through micro- or nanochannels is to modify the no-slip boundary condition in continuum models by accounting for a slip boundary condition. This approach has been used in multiple proposed models for shale gas transport (Javadpour 2009; Civan 2010; Azom and Javadpour 2012; Darabi et al. 2012).

Javadpour (2009) proposed a model that includes the Knudsen diffusion and the slip flow which are major mechanisms contributing to the gas flow in a single, straight, cylindrical nanotube. Javadpour also asserted that these two processes exist at any  $K_n$ , but their individual contributions to total flux varies. Javadpour (2009) proposed a model for gas flow in a nanopore duct by accounting for Knudsen diffusion and slip velocity using the Maxwell theory.

$$J = \left[ \frac{2rM}{3 \times 10^3 RT} \left( \frac{8RT}{\pi M} \right)^{0.5} + F \frac{r^2 \rho_{\text{avg}}}{8\mu} \right] \frac{p_2 - p_1}{L} \quad (2.14)$$

where  $J$  is the mass flux or molar flux,  $r$  the pore radius,  $M$  the molar mass,  $F$  the slip coefficient,  $\rho_{\text{avg}}$  the average density, and  $L$  the length of the media.  $p_1$  and  $p_2$  are the upstream and downstream pressures respectively. The first and second terms in the right-hand-side bracket in Eq. 2.14 refer to Knudsen diffusion and slip flow, respectively. The term  $F$  is the slip coefficient and is defined as:

$$F = 1 + \left( \frac{8\pi RT}{M} \right)^{0.5} \frac{\mu}{rp_{\text{avg}}} \left( \frac{2}{\alpha} - 1 \right) \quad (2.15)$$

where the  $\alpha$  is the tangential momentum accommodation coefficient or the fraction of gas molecules reflected diffusely from the pore wall relative to specular reflection. The value of  $\alpha$  varies theoretically in a range from 0 (representing specular accommodation) to 1 (representing diffuse accommodation), depending on wall-surface smoothness, gas type, temperature, and pressure (Agrawal and Prabhu 2008; Arkilic et al. 2001). Experimental measurements are needed to determine  $\alpha$  for specific shale systems.

Javadpour (2009) showed that this model matches data by Roy et al. (2003), from flow through a membrane with pore sizes of 200 nm, at an average error of 4.5 %. By comparing Eq. 2.14 to Darcy's law for a single nanotube (Hagen-Poiseuille equation), apparent permeability,  $k_{\text{app}}$ , for a porous medium containing of straight cylindrical nanotubes can be defined as:

$$k_{\text{app}} = \frac{2r\mu}{3 \times 10^3 p_{\text{avg}}} \left( \frac{8RT}{\pi M} \right)^{0.5} + \frac{r^2}{8} \left\{ 1 + \left( \frac{8\pi RT}{M} \right)^{0.5} \left( \frac{2}{\alpha} - 1 \right) \frac{\mu}{rp_{\text{avg}}} \right\} \quad (2.16)$$

where  $k_{\text{app}}$  apparent permeability. Equation 2.16 provides an apparent Darcy permeability relationship written in the Klinkenberg form as

$$k_{\text{app}} = k_D \left( 1 + \frac{b}{p_{\text{avg}}} \right) \quad (2.17)$$

$$b = \frac{16\mu}{3 \times 10^3 r} \left( \frac{8RT}{\pi M} \right)^{0.5} + \left( \frac{8\pi RT}{M} \right)^{0.5} \left( \frac{2}{\alpha} - 1 \right) \frac{\mu}{r}, \quad (2.18)$$

Azom and Javadpour (2012) showed how Eq. 2.16 can be corrected for a real gas flowing in a porous medium. The final equation still has the form of Eq. 2.17, but with  $b$  given below

$$b = \frac{16\mu c_g p_{\text{avg}}}{3 \times 10^3 r} \left( \frac{8ZRT}{\pi M} \right)^{0.5} + \left( \frac{8\pi RT}{M} \right)^{0.5} \left( \frac{2}{\alpha} - 1 \right) \frac{\mu}{r}, \quad (2.19)$$

where  $c_g$  is gas compressibility and  $Z$  is compressibility factor. Notice that as the real gas becomes ideal, Eq. 2.19 becomes Eq. 2.18, because the gas compressibility  $c_g = \frac{1}{p_{\text{avg}}}$  and the compressibility factor  $z = 1$  for an ideal gas.

Darabi et al. (2012) later applied several modifications to adapt the model developed by Javadpour (2009) from being applicable to a single, straight, cylindrical nanotube to being applicable to ultra-tight, natural porous media characterized by a network of inter-connected tortuous micropores and nanopores. This model accounts for Knudsen diffusion and surface roughness, in addition to slip flow, by use of the Maxwell theory.

$$k_{\text{app}} = \frac{\mu M \phi}{RT \tau \rho_{\text{avg}}} (\delta_r)^{D_f - 2} D_k + k_D \left( 1 + \frac{b}{p_{\text{avg}}} \right). \quad (2.20)$$

In Eq. 2.20,  $\tau$  is the tortuosity and  $\delta_r$  the ratio of normalized molecular radius size,  $r_m$ , with respect to local average pore radius,  $r_{\text{avg}}$ , yielding  $\delta_r = \frac{r_m}{r_{\text{avg}}}$ . In above equation, Knudsen diffusion coefficient,  $D_k$ , is defined as

$$D_k = \frac{2r_{\text{avg}}}{3} \left( \frac{8RT}{\pi M} \right)^{0.5}, \quad (2.21)$$

where  $r_{\text{avg}}$  is approximated by  $r_{\text{avg}} = (8k_D)^{0.5}$ . The average pore radius can also be determined by laboratory experiments employing such as processes as mercury injection and nitrogen adsorption tests and pore imaging using SEM and AFM.

Darabi et al. (2012) also included the fractal dimension of the pore surface,  $D_f$ , to consider the effect of pore-surface roughness on the Knudsen diffusion coefficient (Coppens 1999; Coppens and Dammers 2006). Surface roughness is one example of local heterogeneity. Increasing surface roughness leads to an increase in

residence time of molecules in porous media and a decrease in Knudsen diffusivity.  $D_f$  is a quantitative measure of surface roughness that varies between 2 and 3, representing a smooth surface and a space-filling surface, respectively (Coppens and Dammers 2006).

Civan (2010) permeability model is based on the Beskok and Karniadakis (1999) approach. The model represented by simplified second-order slip approach assumes that permeability is a function of the intrinsic permeability, the Knudsen number,  $K_n$ , the rarefaction coefficient  $\alpha_r$ , and the slip coefficient  $b$ ,

$$k = k_D(1 + \alpha_r K_n) \left( 1 + \frac{4K_n}{1 - bK_n} \right). \quad (2.22)$$

The dimensionless rarefaction coefficient  $\alpha_r$  is given by,

$$\alpha_r = \alpha_0 \left( \frac{K_n^B}{A + K_n^B} \right). \quad (2.23)$$

where  $A$  and  $B$  are empirical fitting constants. The lower limit of  $\alpha_r$  ( $\alpha_r = 0$ ) corresponds to the slip flow regime and the upper limit  $\alpha_0$  corresponds to the asymptotic limit of  $\alpha_r$  when  $K_n \rightarrow \infty$ , which corresponds to the free molecular flow. Constants  $A$  and  $B$  serve as the fitting parameters that may be appropriately adjusted based on the dominant flow regime in the shale porous media. Civan (2010) reports the adjusted parameter values,  $A = 0.178$ ,  $B = 0.4348$ , and  $\alpha_0 = 0.1358$  for modeling gas flow in a tight sand example. Civan (2010) assumes  $b = -1$  based on the Beskok and Karniadakis (1999) estimate and subsequently estimates the Knudsen number as (Jones and Owens 1980),

$$K_n = 12.639 k_D^{-1/3}. \quad (2.24)$$

With these assumptions, the only unknown parameter remaining in the Civan (2010) model is  $k_D$ , which can be determined from a permeability measurement experiment (e.g., the pulse-decay experiment).

For small Knudsen numbers, that is,  $K_n \ll 1$ , Civan (2010) estimates the dynamic slippage coefficient  $b_k$  as a function of gas viscosity, based on the Florence et al. (2007)'s study,

$$b_k = \frac{2790\mu}{\sqrt{M}} \left( \frac{k_D}{\phi} \right)^{-0.5}. \quad (2.25)$$

The most important limitation to these discussed models is the estimation of empirical parameters which requires performing experiments or computationally expensive molecular-dynamic simulations (Agrawal and Prabhu 2008). Singh et al. (2014) proposed a new non-empirical, analytical model for permeability, termed non-empirical apparent permeability (NAP). NAP is developed for flow of gas in

ultra-tight porous media consisting of tortuous micro-/nano-pores and is valid for Knudsen numbers less than unity and stands up under the complete operating conditions of shale reservoirs.

Singh et al. (2014) derived apparent permeability on the basis of fundamental flow equations for shale-gas systems. From the total mass flow which is a superposition of advection and molecular spatial diffusion (Veltzke and Thöming 2012), Darcy's law can be converted to expressions for apparent permeability of slits or tubes:

$$(k_{\text{app}})_{\text{slit}} = \frac{\phi \mu h}{3\tau} \left( \frac{h_{\text{slit}} Z}{4\mu} \frac{8}{\pi p_{\text{avg}} M} \sqrt{\frac{2MRT}{\pi}} \right) \quad (2.26)$$

$$(k_{\text{app}})_{\text{tube}} = \frac{2\phi \mu d}{\pi \tau} \left( \frac{\pi d_{\text{tube}} Z}{64\mu} \frac{1}{3p_{\text{avg}} M} \sqrt{2\pi MRT} \right) \quad (2.27)$$

where  $h_{\text{slit}}$  is the height of the rectangular slit and  $d_{\text{tube}}$  the diameter of the tube. The two pore geometries considered in the NAP model are cylindrical tube and rectangular channel (slit). When porous media are composed of other shapes, the permeability of the media will be somewhere between what it would be if it were composed of tubes and what it would be if it were composed of slits. Therefore, the two shapes considered in the NAP model may reliably capture the average effect of different pore shapes in porous media because capturing the exact shape of each pore might be impractical and daunting. The permeability of each shape type contributes to the effective permeability of the reservoir, where the effective permeability is the statistical sum of the individual permeability from each shape type (Fenton 1960) as given below:

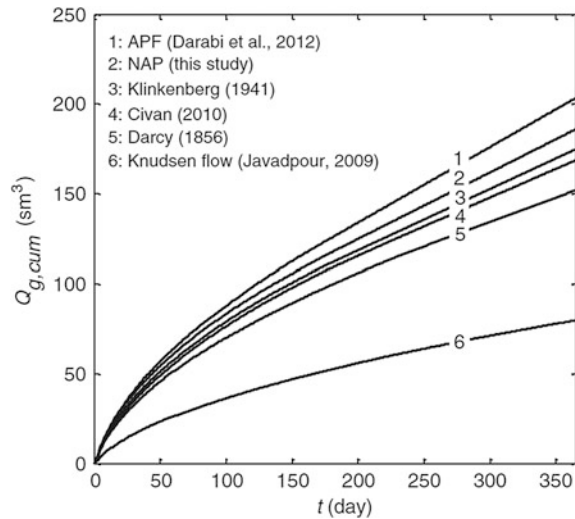
$$\ln(k_{\text{app}})_{\text{eff}} = \frac{x}{100} \ln(k_{\text{app}})_{\text{slit}} + \frac{100-x}{100} \ln(k_{\text{app}})_{\text{tube}} \quad (2.28)$$

$$(k_{\text{app}})_{\text{eff}} = \left[ \left( k_{\text{app}}^{\frac{x}{100}} \right)_{\text{slit}} \left( k_{\text{app}}^{\frac{100-x}{100}} \right)_{\text{tube}} \right] \quad (2.29)$$

where  $k_{\text{eff}}$  is effective permeability after including the effect of sorption. The novelty of this work is the development of flow equations without empirical parameters. Although there are some empirical values of simple gases and solid materials in literature, finding them for the shale system is not straightforward. Hence, a method that does not need the empirical value is attractive.

Figure 2.7 compares the predictions of cumulative gas production for the APF (Darabi et al. 2012), NAP (Singh et al. 2014), Klinkenberg (1941), Civan (2010), Darcy-type-flow, and Knudsen-diffusion models (Javadpour 2009). The NAP predictions lie between APF and Klinkenberg, whereas Civan and Klinkenberg predictions are close to each other and each of them is higher than the predictions by Darcy. At the given typical shale-gas-reservoir conditions, contribution of Darcy flow, slip flow, and Knudsen diffusion control total gas production. The APF model

**Fig. 2.7** Comparison of different gas models to predict cumulative gas production (Singh et al. 2014)

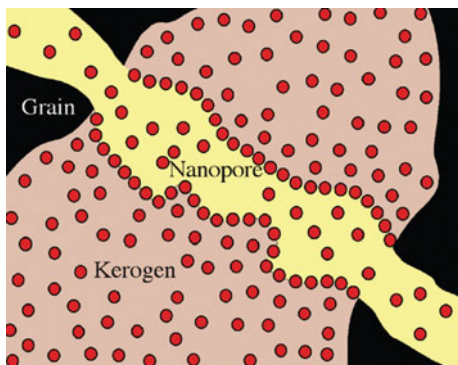


includes all these three processes, whereas the NAP model ignores slip flow. A comparison between APF (Darabi et al. 2012) and NAP model in Fig. 2.7 suggests that the Klinkenberg effect is not dominant at high-Knudsen-number flow (applicable to shale gas) and that a combination of Darcy-type flow corrected for Knudsen diffusion can be used alternatively.

As mentioned earlier in this chapter, gas storage in gas shale exists in three major forms: stored as compressed gas in the pore network, sorbed on the surface of organic material and possibly on clay minerals, and dissolved in liquid hydro-carbon and brine (interstitial and clay-bound), and kerogen (Javadpour et al. 2007). Many research studies have addressed the first two storage processes (Chareonsuppanimit et al. 2012; Civan et al. 2012; Darabi et al. 2012; Javadpour 2009; Zhang et al. 2012), but only limited research has been conducted on the contribution of gas dissolved in organic material in the total gas production from shale reservoirs (Etminan et al. 2014; Moghanloo et al. 2013).

Figure 2.8 shows the gas-molecule in a part of pore system including kerogen. The compressed gas exists in the micro- and nano-scale pores. Some of the gas molecules are adsorbed on the surface of kerogen and, eventually, some of the gas molecules are dissolved into the kerogen body and become a part of the kerogen in the form of a single phase. The controlling mass transport process of the dissolved gas is molecular diffusion. Depending on the geochemistry of the organic materials (thermal maturity, organic source, etc.), different gas solubility could be expected. The contribution of dissolved gas to gas-in-place and ultimate recovery of a shale reservoir could be significant; hence, evaluation of the gas-diffusion process into kerogen becomes important. In addition to the total contribution of each process, the onset time of each process during production is critical. Once production starts from a reservoir, the compressed gas in interstitial pore spaces expands first; then, adsorbed gas on the surfaces of the pores in kerogen desorbs to the pore network.

**Fig. 2.8** Schematic view of gas-molecule locations in a small part of pore system including kerogen (Javadpour 2009)



At this stage, the concentration of gas molecules on the pore inner surface decreases and creates a concentration gradient in the bulk of the kerogen, thereby triggering gas diffusion (Etminan et al. 2014; Javadpour et al. 2007).

## 2.5 Non-Darcy Flow

In 1856, Darcy developed his now famous flow correlation by flowing water, available at the local hospital, through sand pack configurations. Darcy's law, shown in Eq. 2.30, describes the linear proportionality involving a constant,  $k$ , as related to the potential gradient  $\frac{dp}{dx}$ , the fluid viscosity of  $\mu$ , and the superficial velocity of  $v$ .

$$-\frac{dp}{dx} = \frac{\mu v}{k} \quad (2.30)$$

where  $v$  is the superficial velocity. Forty-five years later, Forchheimer (1901) observed deviation from the linearity of Darcy's equation at increased flow rates. When the gas velocity increases, for example near the drain inside hydraulic fractures, significant inertial (non-Darcy) effects can occur. This induces an additional pressure drop in the hydraulic fractures in order to maintain the production rate. Forchheimer proposed a second proportionality constant, in addition to  $k$ , that would account for this non-linearity. He called this second proportionality constant,  $\beta$ , and it resulted in the familiar Forchheimer equation shown in Eq. 2.31.

$$-\frac{dp}{dx} = \frac{\mu v}{k} + \beta \rho v^2 \quad (2.31)$$

where  $\beta$  is the non-Darcy flow coefficient. The earliest references to non-Darcy flow effects in petroleum literature occur in the early 1960s (Carter 1962; Swift and

Kiel 1962; Tek et al. 1962). The effects of non-Darcy flow specifically in hydraulic fracturing operations were first addressed by Cooke (1973) as given below:

$$\beta = bk^{-a} \quad (2.32)$$

where  $a$  and  $b$  are constant determined by experiments based on proppant type. Equation 2.32 is simple and applicable to different types of proppants.

Geertsma (1974) developed a dimensionally consistent correlation between the non-Darcy flow coefficient, permeability and porosity. Analyzing the data obtained for unconsolidated sandstones, consolidated sandstones, limestones, and dolomites from his and other experiments (Green and Duwez 1951; Cornell and Katz 1953) and performed dimensional analysis, he reached an empirical correlation,

$$\beta = \frac{0.005}{\phi^{5.5}k^{0.5}}. \quad (2.33)$$

In addition to the one phase correlation Eq. 2.33, Geertsma (1974) proposed a correlation for  $\beta$  in a two-phase system. He argued that, in the two-phase system, the permeability in Eq. 2.33 would be replaced by the gas effective permeability at a certain water saturation, while the porosity would be replaced by the void fraction occupied by the gas. Therefore, in the two-phase system, where the fluid was immobile, the  $\beta$  correlation became

$$\beta = \frac{0.005}{\phi^{5.5}k^{0.5}} \left[ \frac{1}{(1 - S_{wr})^{5.5}k_r^{0.5}} \right]. \quad (2.34)$$

where  $S_{wr}$  is the residual water saturation and  $k_r$  is the relative permeability. Equation 2.34 shows that the presence of the liquid phase increases the non-Darcy coefficient.

Evans and Civan (1994) presented a general correlation for the non-Darcy flow coefficient using a large variety of data from consolidated and unconsolidated media including the effects of multiphase fluids and overburden stress. They collected a total of 183 data points and also employed data from Geertsma (1974) in consolidated media, and from Evans and Evans (1988) for the effects of immobile liquid saturation and closure stress on the  $\beta$ -coefficient in propped fractures. The regression line yielded the following general correlation:

$$\beta = \frac{1.485 \times 10^9}{\phi k^{1.021}} \quad (2.35)$$

with correlation coefficient  $R = 0.974$ . Since this correlation is obtained from a large variety of porous media under different conditions, it is expected to provide a reasonable estimation for the  $\beta$ -coefficient. Equation 2.35 is implemented in the numerical model and used for accounting for non-Darcy flow in hydraulic fractures.

In addition to this correlation, there are several theoretical and empirical correlations of the non-Darcy coefficient in literatures and these are reviewed by Evans and Civan (1994) and Dacun and Thomas (2001).

## 2.6 Stress-Dependent Compaction

In shale formations, the conductivity of fracture network is sensitive to the change in stress and strain during production because natural fractures are weakly propped compared with hydraulic fractures. Figure 2.9 shows that experimental results measuring permeability and porosity with respect to effective confining pressure (Dong et al. 2010). Therefore, geomechanical effects during production must be included to simulate the stress-dependent effects of shale gas reservoir.

Previous researches successfully proved that iterative coupling between geomechanics and reservoir flow allows easy control of convergence as well as easy maintenance of the reservoir and geomechanics simulators (Tran et al. 2005, 2010). However, it is concluded that linear elastic model cannot solely describe shale gas reservoirs (Li and Ghassemi 2012; Hosseini 2013). In order to consider the change of conductivity, pressure-dependent properties were presented in several researches (Pedrosa 1986; Raghavan and Chin 2004; Cho et al. 2013). Therefore, the deformation of shale reservoir should be modeled by stress-dependent correlations coupled with linear-elastic model. To consider decreasing production caused by porosity and permeability reduction in the shale gas reservoir model, stress-dependent porosity and permeability correlations are applied with a linear elastic constitutive model. Dong et al. (2010) used exponential and power law correlations to match the experimental data as follows:

$$\phi = \phi_i e^{-a(\sigma' - \sigma'_i)} \quad (2.36)$$

$$k = k_i e^{-b(\sigma' - \sigma'_i)} \quad (2.37)$$

$$\phi = \phi_i \left( \frac{\sigma'}{\sigma'_i} \right)^{-c} \quad (2.38)$$

$$k = k_i \left( \frac{\sigma'}{\sigma'_i} \right)^{-d} \quad (2.39)$$

where  $\sigma'$  is the effective stress and  $a$ ,  $b$ ,  $c$ , and  $d$  are experimental coefficients. The subscript  $i$  indicates the initial state. Figure 2.10 shows that results of curve fitting on measured porosity and permeability of the shale cores with exponential and power law correlations (Dong et al. 2010).



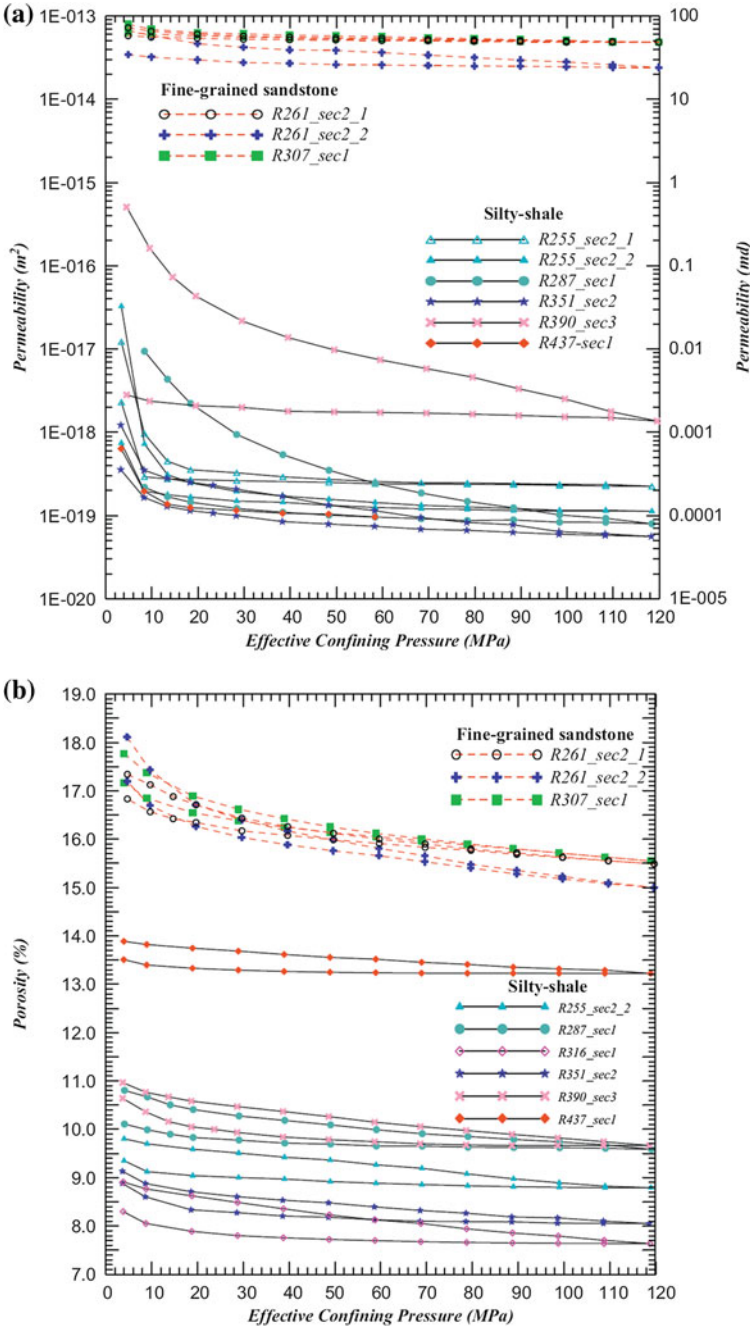


**Fig. 2.9** Stress-dependent **a** permeability and **b** porosity of the sandstone (red dashed lines) and silty-shale (solid black lines) (Dong et al. 2010)

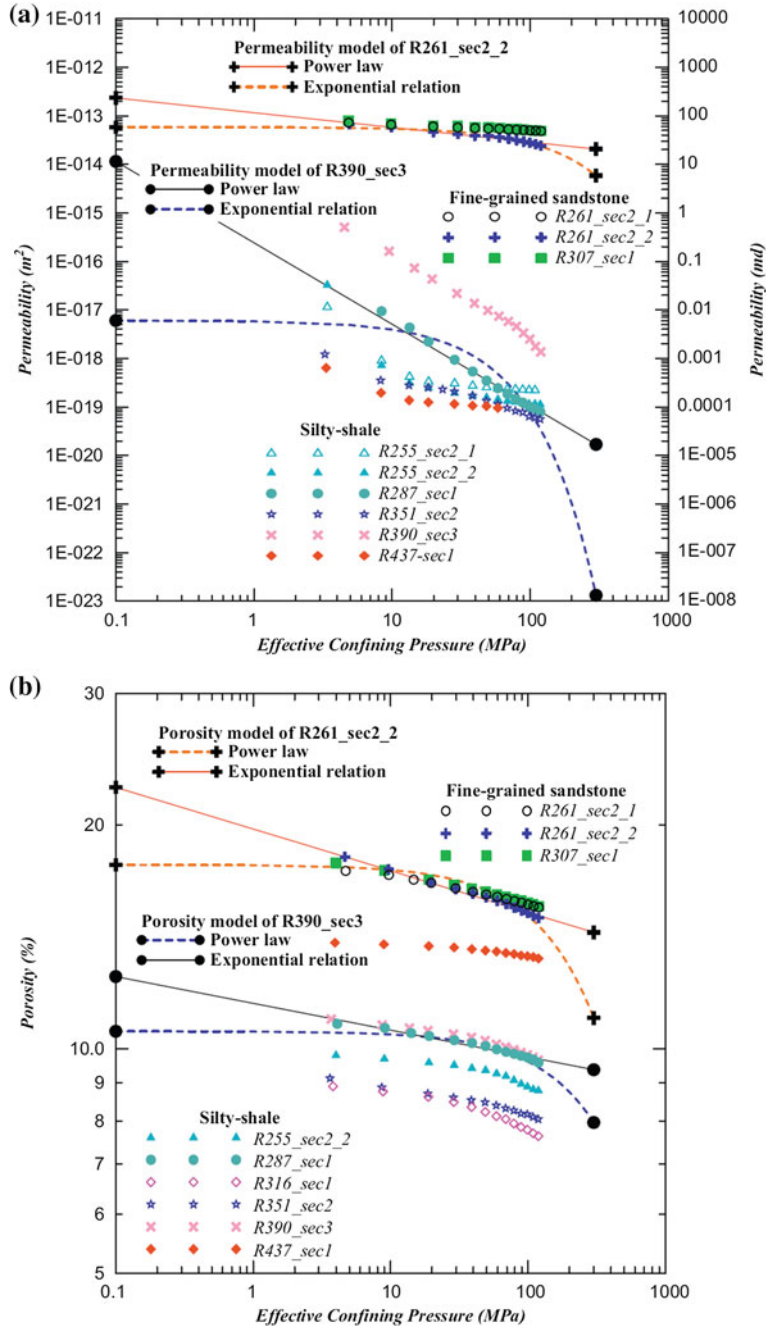


**Fig. 2.10** Comparison between the models adopting a power law and exponential relationship for **a** permeability and **b** porosity (Dong et al. 2010)

## References

- Agrawal A, Prabhu SV (2008) Survey on measurement of tangential momentum accommodation coefficient. *J Vac Sci Technol A* 26(4):634–645. doi:[10.1116/1.2943641](https://doi.org/10.1116/1.2943641)
- Arkilic EB et al (2001) Mass flow and tangential momentum accommodation in silicon micromachined channels. *J Fluid Mech* 437:29–43
- Azom P, Javadpour F (2012) Dual-continuum modeling of shale and tight gas reservoirs. Paper presented at the SPE annual technical conference and exhibition, San Antonio, Texas, 8–10 Oct 2012. doi:[10.2118/159584-MS](https://doi.org/10.2118/159584-MS)
- Barenblatt GI et al (1960) Basic concept in the theory of seepage of homogeneous liquids in fissured rocks. *J Appl Math Mech* 24(5):1286–1303
- Beskok A, Karniadakis GE (1999) A model for flows in channels, pipes, and ducts at micro and nano scales. *Microsc Therm Eng* 3(1):43–77. doi:[10.1080/108939599199864](https://doi.org/10.1080/108939599199864)
- Brown GP et al (1946) The flow of gases in pipes at low pressures. *J Appl Phys* 17:802–813
- Brunauer S et al (1938) Adsorption of gases in multimolecular layers. *J Am Chem Soc* 60(2):309–319
- Carter RD (1962) Solutions of unsteady-state radial gas flow. *J Pet Tech* 14(05):549–554. doi:[10.2118/108-PA](https://doi.org/10.2118/108-PA)
- Chareonsuppanimit P et al (2012) High-pressure adsorption of gases on shales: measurements and modeling. *Int J Coal Geol* 95:34–46. doi:[10.1016/j.coal.2012.02.005](https://doi.org/10.1016/j.coal.2012.02.005)
- Cho Y et al (2013) Pressure-dependent natural-fracture permeability in shale and its effect on shale-gas well production. *SPE Res Eval Eng* 16(2):216–228. doi:[10.2118/159801-PA](https://doi.org/10.2118/159801-PA)
- Civan F (2010) Effective correlation of apparent gas permeability in tight porous media. *Transp Porous Med* 82(2):375–384. doi:[10.1007/s11242-009-9432-z](https://doi.org/10.1007/s11242-009-9432-z)
- Cooke CE (1973) Conductivity of fracture proppants in multiple layers. *J Pet Tech* 25(09):1101–1107. doi:[10.2118/4117-PA](https://doi.org/10.2118/4117-PA)
- Coppens M-O (1999) The effect of fractal surface roughness on diffusion and reaction in porous catalysts from fundamentals to practical applications. *Catal Today* 53(2):225–543. doi:[10.1016/S0920-5861\(99\)00118-2](https://doi.org/10.1016/S0920-5861(99)00118-2)
- Coppens M-O, Dammers AJ (2006) Effects of heterogeneity on diffusion in nanopores from inorganic materials to protein crystals and ion channels. *Fluid Phase Equilibr* 241(1–2):308–316. doi:[10.1016/j.fluid.2005.12.039](https://doi.org/10.1016/j.fluid.2005.12.039)
- Cornell D, Katz DL (1953) Flow of gases through consolidated porous media. *Ind Eng Chem* 45(10):2145–2152. doi:[10.1021/ie50526a021](https://doi.org/10.1021/ie50526a021)
- Dacun L, Thomas WE (2001) Literature review on correlations of the non-darcy coefficient. Paper presented at the SPE Permian basin oil and gas recovery conference, Midland, Texas, 15–17 May 2001. doi:[org/10.2118/70015-MS](https://doi.org/10.2118/70015-MS)
- Darabi H et al (2012) Gas flow in ultra-tight shale strata. *J Fluid Mech* 710:641–658. doi:[10.1017/jfm.2012.424](https://doi.org/10.1017/jfm.2012.424)
- Dong JJ et al (2010) Stress-dependence of the permeability and porosity of sandstone and shale from TCDP Hole-A. *Int J Rock Mech Min Sci* 47(7):1141–1157. doi:[10.1016/j.ijrmms.2010.06.019](https://doi.org/10.1016/j.ijrmms.2010.06.019)
- Etmiman SR et al (2014) Measurement of gas storage processes in shale and of the molecular diffusion coefficient in kerogen. *Int J Coal Geol* 123:10–19. doi:[10.1016/j.coal.2013.10.007](https://doi.org/10.1016/j.coal.2013.10.007)
- Evans EV, Evans RD (1988) The influence of an immobile or mobile saturation on non-Darcy compressible flow of real gases in propped fractures. *J Pet Tech* 1345–1351. doi:[10.2118/15066-PA](https://doi.org/10.2118/15066-PA)
- Evans RD, Civan F (1994) Characterization of non-darcy multiphase flow in petroleum bearing formation. U.S. Department of Energy, Washington, D.C
- Fenton L (1960) The sum of log-normal probability distributions in scatter transmission systems. *IEEE T Commun* 8(1):57–67. doi:[10.1109/TCOM.1960.1097606](https://doi.org/10.1109/TCOM.1960.1097606)

- Florence FA et al (2007) Improved permeability prediction relations for low-permeability sands. Paper presented at SPE Rocky mountain oil and gas technology symposium, Denver, Colorado, 16–18 April 2007
- Forchheimer P (1901) Wasserbewegung durch boden. *Zeits V Deutsch Ing* 45:1781–1901
- Freeman CM et al (2012) Measurement, modeling, and diagnostics of flowing gas composition changes in shale gas wells. Paper presented at the SPE Latin American and Caribbean petroleum engineering conference, Mexico City, Mexico, 16–18 April 2012
- Gad-el-Hak M (1999) The fluid mechanics of microdevices—the freeman scholar lecture. *J Fluids Eng* 121(1):5. doi:[10.1115/1.2822013](https://doi.org/10.1115/1.2822013)
- Gao C et al (1994) Modeling multilayer gas reservoirs Including sorption effects. Paper presented at the SPE eastern regional conference and exhibition, Charleston, West Virginia, 8–10 Nov 1994
- Geertsma J (1974) Estimating the coefficient of inertial resistance in fluid flow through porous media. *Soc Pet Eng J* 14(05):445–450. doi:[10.2118/4706-PA](https://doi.org/10.2118/4706-PA)
- Green L, Duwez PJ (1951) Fluid flow through porous metals. *J Appl Mech* 18(1):39
- Hosseini SM (2013) On the linear elastic fracture mechanics application in Barnett shale hydraulic fracturing. Paper presented at the 47th U.S. rock mechanics/geomechanics symposium, San Francisco, California, 23–26 June 2013
- Javadpour F (2009) Nanopores and apparent permeability of gas flow in mudrocks (shales and siltstone). *J Can Pet Tech* 48(8):16–21. doi:[10.2118/09-08-16-DA](https://doi.org/10.2118/09-08-16-DA)
- Javadpour F et al (2007) Nanoscale gas flow in shale gas sediments. *J Can Pet Tech* 46(10):55–61. doi:[10.2118/07-10-06](https://doi.org/10.2118/07-10-06)
- Jones FO, Owens WW (1980) A laboratory study of low-permeability gas sands. *J Pet Technol* 32(9):1631–1640
- Klinkenberg LJ (1941) The permeability of porous media to liquids and gases. In: *Drilling and production practice*, New York, New York, January 1941
- Kuila U, Prasad M (2013) Specific surface area and pore-size distribution in clays and shales. *Geophys Prosp* 61(2):341–362
- Langmuir I (1918) The adsorption of gases on plane surfaces of glass, mica and platinum. *J Am Chem Soc* 40:1403–1461
- Li Y, Ghassemi A (2012) Creep behavior of Barnett, Haynesville, and Marcellus shale. Paper presented at the 46th U.S. rock mechanics/geomechanics symposium, Chicago, Illinois, 24–27 June 2012
- Moghanloo RG et al (2013) Contribution of methane molecular diffusion in kerogen to gas-in-place and production. Paper presented at the SPE western regional and AAPG pacific section meeting 2013 Joint technical conference, Monterey, California, 19–25 April. doi:[10.2118/165376-MS](https://doi.org/10.2118/165376-MS)
- Pedrosa OA (1986) Pressure transient response in stress-sensitive formations. Paper presented at the SPE California regional meeting, Oakland, California, 2–4 April 1986. doi:[10.2118/15115-MS](https://doi.org/10.2118/15115-MS)
- Raghavan R, Chin LY (2004) Productivity changes in reservoirs with stress-dependent permeability. *SPE Res Eval Eng* 7(4):308–315. doi:[10.2118/88870-PA](https://doi.org/10.2118/88870-PA)
- Rathakrishnan E (2004) Gas dynamics. Prentice-hall of India Pvt Ltd, New Delhi, India
- Rezaee R (eds) (2015) *Fundamental of gas shale reservoirs*. Wiley, New Jersey
- Roy S et al (2003) Modeling gas flow through microchannels and nanopores. *J Appl Phys* 93:4870–4879. doi:[10.1063/1.1559936](https://doi.org/10.1063/1.1559936)
- Shabro V et al (2012) Finite-difference approximation for fluid-flow simulation and calculation of permeability in porous media. *Transport Porous Med* 94(3):775–793. doi:[10.1007/s11242-012-0024-y](https://doi.org/10.1007/s11242-012-0024-y)
- Silin D, Kneafsey T (2012) Shale gas: nanometer-scale observations and well modeling. *J Can Pet Tech* 51(6):464–475
- Sing KSW et al (1985) Reporting physisorption data for gas/solid systems with special reference to the determination of surface area and porosity. *Pure Appl Chem* 57(4):603–619
- Singh H et al (2014) Nonempirical apparent permeability of shale. *SPE Res Eval Eng* 17(3):414–424. doi:[10.2118/170243-PA](https://doi.org/10.2118/170243-PA)
- Stewart G (2011) *Well test design and analysis*. Pennwell, Tulsa, Oklahoma

- Swift GW, Kiel OG (1962) The prediction of gas-well performance including the effect of non-darcy flow. *J Pet Tech* 14(07):791–798. doi:[10.2118/143-PA](#)
- Tek MR et al (1962) The effect of turbulence on flow of natural gas through porous reservoirs. *J Pet Tech* 14(07):799–806. doi:[10.2118/147-PA](#)
- Tran D et al (2005) An overview of iterative coupling between geomechanical deformation and reservoir flow. Paper presented at the SPE international thermal operations and heavy oil symposium, Calgary, Alberta, Canada, 1–3 Nov 2005. doi:[10.2118/97879-MS](#)
- Tran D et al (2010) Improved gridding technique for coupling geomechanics to reservoir flow. *Soc Pet Eng J* 15(1):64–75. doi:[10.2118/115514-PA](#)
- Veltzke T, Thöming J (2012) An analytically predictive model for moderately rarefied gas flow. *J Fluid Mech* 698:406–422. doi:[10.1017/jfm.2012.98](#)
- Warren JE, Root PJ (1963) The behavior of naturally fractured reservoirs. *Soc Petrol Eng J* 3(3):245–255
- Yu W et al (2014) Evaluation of gas adsorption in Marcellus shale. Paper presented at the SPE annual technical conference and exhibition, Amsterdam, The Netherlands, 27–29 Oct 2014
- Zhang T et al (2012) Effect of organic-matter type and thermal maturity on methane adsorption in shale gas systems. *Org Geochem* 47:120–131. doi:[10.1016/j.orggeochem.2012.03.012](#)

Integrative Understanding of Shale Gas Reservoirs

Lee, K.S.; Kim, T.H.

2016, XI, 123 p. 82 illus., 5 illus. in color., Softcover

ISBN: 978-3-319-29295-3